Laser Spectroscopic Excitation Function and Reaction Threshold Studies of the H + DCl → HCl + D Gas-Phase Isotope Exchange Reaction†

Almuth Läuter, Rajesh K. Vatsa,‡ Jai P. Mittal, Hans-Robert Volpp,* and Jürgen Wolfrum

Physikalisch-Chemisches Institut der Universität Heidelberg, Im Neuenheimer Feld 253, D-69120 Heidelberg, Germany

Received: August 25, 2005; In Final Form: December 8, 2005

The dynamics of the gas-phase hydrogen atom exchange reaction H + DCl → HCl + D were studied using the pulsed laser photolysis/laser induced fluorescence "pump-and-probe" method. Laser photolysis of H_2S at 222 nm was used to generate nonequilibrium distributions of translationally excited hydrogen atoms at high dilution in a flowing moderator gas (Ar)/reagent (DCl) mixture. H and D atoms were detected with sub-Doppler resolution via Lyman-α laser induced fluorescence spectroscopy, which allowed the measurement of the line shapes of the moderated H atom Doppler profiles as well as the concentration of the D atoms produced in the H + DCl → HCl + D reaction. From the measured H atom Doppler profiles, the time evolution of the initially generated nascent nonequilibrium H atom speed distribution toward its room-temperature thermal equilibrium form was determined. In this way, the excitation function and the reaction threshold ($E_0 = 0.65 \pm 0.13$ eV) for the H + DCl → HCl + D reaction could be determined from the measured nonequilibrium D atom formation rates and single collision absolute reaction cross-section values of 0.12 ± 0.04 Å^2 and 0.45 ± 0.11 Å^2 measured at reagent collision energies of 1.0 and 1.4 eV, respectively.

I. Introduction

Since the pioneering experimental work of Bodenstein and Dux on the photochemical kinetics of the hydrogen−chlorine system,[1,2] the elementary reactions

$$H + HCl \rightarrow H_2 + Cl \quad (1)$$

$$H + HCl \rightarrow HCl + H \quad (2)$$

and the reverse reaction Cl + H_2 (reaction −1) have played seminal roles in the evolution of modern chemical kinetics and reaction dynamics.[3] Reaction 1 represents the H atom abstraction channel, while reaction 2 represents the H atom exchange channel of the HClH reactive system. Great efforts have been made in recent years to construct an accurate global potential energy surface (PES) required for the theoretical investigation of reactions 1, −1, and 2.[3−5]

A large number of experimental thermal kinetics studies were carried out for the reactions 1 and −1, resulting in quite accurate Arrhenius parameters for the thermal rate coefficients in the temperature ranges 195−1200 K and 199−3020 K, respectively.[6,7] The results of the latter kinetics studies were found to be in generally good agreement with the results of rate constant calculations[8−10] on the G3 PES.[4] The G3 PES was also employed, along with the more recently developed BW1 and BW2 PESs,[5] in comparative quasi-classical trajectory (QCT) studies in which reaction cross-sections for reactions 1 and 2 as well as for the hydrogen atom abstraction (reaction 3) and hydrogen atom exchange (reaction 4) reactions of the isotopic variant H + DCl were calculated for reagent collision energies from the reaction threshold up to $E_{c.m.} = 2.4$ eV.[11,12]

$$H + DCl \rightarrow HD + Cl \quad (3)$$

$$H + DCl \rightarrow HCl + D \quad (4)$$

In a subsequent theoretical study, quantum mechanical scattering (QMS) calculations were performed on the BW2 PES in which reaction cross-sections for reactions 1 and 2 in the collision energy range $E_{c.m.} = 0.1-1.4$ eV were computed.[13] On the experimental side, several reaction cross-section measurements were performed for the abstraction reaction 1 in which translationally excited H atoms were employed in combination with state-resolved detection of H_2 product molecules using coherent anti-Stokes Raman scattering (CARS)[14] and vacuum ultraviolet laser induced fluorescence (VUV-LIF) detection of ground-state Cl($^2P_{3/2}$) atom products, respectively.[12,15] The results of the latter VUV-LIF absolute reactive cross-section measurements, which agreed reasonably well with the results of QCT calculations on the G3 PES,[11,12] demonstrated that there is no sharp increase in the reaction cross-section of reaction 1 in the collision energy range $E_{c.m.} = 1.0-1.7$ eV, as was suggested by the earlier CARS experiments.[14] Experimental studies of reaction 3, in which resonance-enhanced multiphoton ionization (REMPI)[16] and VUV-LIF spectroscopy[17] were utilized for ground-state Cl($^2P_{3/2}$) atom product detection, yielded reaction cross-sections which were found to be in good agreement with the results of QCT calculations on the G3 PES.[11,12] In further experiments, VUV-LIF spectroscopy could be successfully applied for the detection of spin−orbit excited Cl*($^2P_{1/2}$) atoms formed via a nonadiabatic reaction pathway in the H + HCl and H + DCl abstraction reactions 1 and 3.[17] In these studies, it was found that the [Cl*]/[Cl + Cl*] spin−orbit product branching ratio in reactions 1 and 3 increases from 6% to 19% and 16%, respectively, in the collision energy range

† Part of the special issue "Jürgen Troe Festschrift".

* Corresponding author. E-mail: aw2@ix.urz.uni-heidelberg.de.

‡ Present address: Novel Material and Structural Chemistry Division, Bhabha Atomic Research Centre, Mumbai, 400085, India.

10.1021/jp054818o CCC: $33.50
Published on Web 02/07/2006

$E_{c.m.} = 1.0-1.7$ eV, demonstrating the increasing importance of the nonadiabatic reaction pathways with increasing collision energy.

The influence of the $Cl^*(^2P_{1/2})$ spin−orbit excited state on the reactivity of the $Cl + H_2/D_2/HD$ abstraction reactions was investigated in the reagent collision energy range $E_{c.m.} = 0.1-0.3$ eV employing a crossed molecular beam apparatus.[18−20] The latter integral reaction cross-section measurements revealed an exceptionally large reactivity for the reactions of $Cl^*(^2P_{1/2})$ atoms, indicating a large extent of electronic nonadiabaticity in these reactions. On the theoretical side, detailed state-of-the-art electronic structure calculations were performed along with exact multielectronic-state QMS calculations,[21] which explicitly allowed for the effect of electronic nonadiabaticity,[22] to rationalize the experimental observations reported in refs 18−20. The QMS calculations of ref 21 revealed an electronically nonadiabatic effect in the $Cl + H_2$ reaction, resulting in an reduction of the reactivity of the ground-state $Cl(^2P_{3/2})$ atom via an electronically nonadiabatic transition in the reactant entrance valley which leads to nonreactive inelastic "backscattering" to the $Cl(^2P_{3/2}) + H_2$ reactants. However, for the elevated collision energies as employed in the experiments,[18−20] the QMS calculations did not yield any indication for the experimental observation of the $Cl^*(^2P_{1/2})$ spin−orbit excited state being substantially more reactive than the $Cl(^2P_{3/2})$ ground state, which is the one which in the $Cl + H_2$ reaction system correlates adiabatically with the observed $HCl + H$ products in their respective ground electronic states. In agreement with most recent $Cl(^2P_{3/2,1/2}) + H_2$ crossed molecular beam measurements of differential cross-sections at elevated[23] and low[24] collision energies, the multi-electronic-state QMS calculations performed on the newly developed CW PESs[25] clearly demonstrated that at all but the very lowest collision energies both integral and differential cross-sections for the spin−orbit excited-state reaction $Cl^*(^2P_{1/2}) + H_2$ are much smaller than those of the ground-state reaction $Cl(^2P_{3/2}) + H_2$.

In contrast to the number of experiments performed to elucidate the dynamics of the abstraction reaction pathways, up to now only one experimental study of the dynamics of the hydrogen atom exchange reaction 4 has been reported, in which absolute reaction cross-sections were measured as a function of reagent collision energy in the range $E_{c.m.} = 1.0-2.4$ eV.[16] The latter experimental values, which exhibited a considerable dispersion, indicated a flat dependence on collision energy with a slightly decreasing tendency in the higher-energy regime. In contrast to this behavior, results of QCT calculations on the GQQ PES,[26] which were also performed in the course of the study reported in ref 16, showed a strictly monotonic increase of the reaction cross-section as a function of collision energy that leads, for the highest collision energy of 2.4 eV as employed in the experiments, to considerably larger cross-sections than experimentally observed. A similar discrepancy between experiment and theory is observed if the experimental results of ref 16 are compared with the results of QCT calculations of the excitation function, i.e., the collision energy dependence of the absolute reaction cross-section $\sigma_R(E_{c.m.})$, obtained on the G3, although (see, e.g., lower panel of figure 4 in ref 11) the G3 reaction cross-sections are considerably smaller (by a factor of about 2) than the GQQ ones. Subsequent QCT studies[12] performed on the BW1 and BW2 PESs for collision energies up to $E_{c.m.} = 2.5$ eV yielded excitation functions which also indicated a strictly monotonic increase of the reaction cross-section as a function of collision energy, with the absolute reaction cross-section values being slightly higher than the corresponding ones obtained on the G3 PES. A comparison between the QCT results[11,12] and the experimental results[16] obtained for $E_{c.m.} < 2.4$ eV is shown in the lower panel of figure 5 in ref 12, which reveals that the experimental values are not reproduced by the calculations on either one of the PESs. As a consequence, the available experimental data[16] so far does not allow for a definite assessment of the comparative quality of the PESs employed in the theoretical dynamics studies of the hydrogen exchange reactions 2 and 4.[11−13,16]

In the work presented in the following article, we applied the moderated hot H atom pulsed laser "pump-and-probe" method described in detail in ref 27, which allows, on the basis of a combination of single collision reaction cross-sections, H atom moderation and nonequilibrium D atom formation rate measurements, to determine the reaction threshold and a global representation of the excitation function for the $H + DCl \rightarrow HCl + D$ hydrogen atom exchange reaction 4. The results obtained in the present study can be directly compared with the results obtained in previous theoretical dynamics studies.[11,12,16]

II. Experimental Section

The present studies were performed using the pulsed laser flash photolysis/laser induced fluorescence (LP/LIF) "pump-and-probe" technique in a flow reactor system at room temperature. The experimental arrangement and methodology employed in the present experiments have been described in detail elsewhere.[27,28] Therefore, only specific details relevant to the present investigations will be given in the following.

The measurements were carried out in a flow reactor made of stainless steel, through which H_2S (UCAR, electronic grade, 99.99%)/DCl (Sigma Aldrich, D > 99%) as H atom precursor/reagent mixtures together with the bath gas Ar (99.998%) could be continuously pumped, with a flow rate high enough to ensure renewal of the gas mixture in the cell between two successive photolysis ("pump") laser shots. The flow rates of the H_2S, DCl, and Ar gases were regulated by calibrated mass flow controllers, and the cell pressure was measured by a MKS Baratron.

In the single collision absolute reaction cross-section measurements, no bath gas was used. Typical values for the $[H_2S]$:[DCl] ratios were between 1:2 and 1:3. These experiments were carried out at low total pressure of $p_{tot} = 40-100$ mTorr and at short pump−probe delay times of $\Delta t = 90-200$ ns to avoid translational relaxation of the translationally "hot" H atoms. The moderated hot H atom experiments were carried out in an excess of Ar buffer gas. In these experiments, the total pressure was typically 1.0−1.1 Torr with H_2S and DCl partial pressures of 10 and 80 mTorr, respectively.

In the present studies, translationally excited H atoms with a nonequilibrium velocity distribution were generated by pulsed laser photolysis (with a laser pulse duration of 15−20 ns) of H_2S at two different excimer laser wavelengths of $\lambda_{pump} = 248$ nm and $\lambda_{pump} = 222$ nm. The photodissociation lasers were operated without polarizing elements, and the analysis of the H atom Doppler profiles generated confirmed that the nascent velocity distributions were essentially spatially isotropic. An aperture was used to skim off a homogeneous part of the rectangular excimer laser profiles to provide photolysis beams, which were slightly focused and directed through the flow cell. Photolysis laser intensities employed in the experiments were in the range 2−5 mJ/cm^2. At these laser intensities, a linear dependence of the photolytically produced H atom concentrations on the intensity of the photolysis laser was observed, and no secondary "high-energy" H atoms due to SH photolysis[29] were detectable.

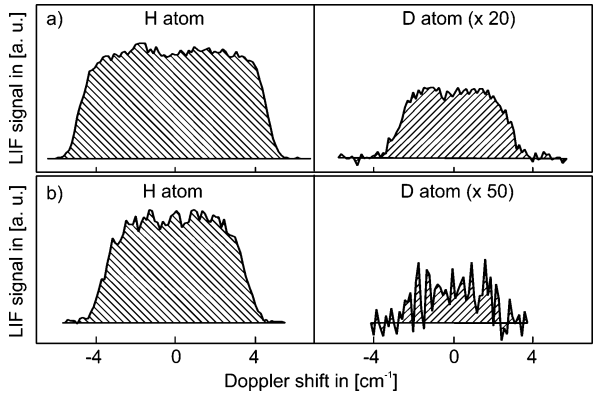

Figure 1. H atom reagent and D atom product Doppler profiles obtained in the H + DCl → HCl + D single-collision reaction cross-section measurements. H atoms with average collision energies of $E_{c.m.}$= 1.4 eV (Figure 1a) and $E_{c.m.}$ = 1.0 eV (Figure 1b) were generated via pulsed laser flash photolysis of H_2S at photolysis laser wavelengths of 222 and 248 nm, respectively, in the presence of 75 mTorr of DCl. D atom products were probed at a delay time of 120 ns. The centers of the Doppler profiles correspond to the Lyman-α transition of the H (82 259.1 cm^{-1}) and D atoms (82 281.4 cm^{-1}), respectively.

H and D atoms were detected by means of Doppler-resolved laser induced fluorescence spectroscopy via the respective ($2p^2$ P ← $1s^2$ S) hydrogen atom Lyman-α transitions. Tunable narrow-band VUV-probe laser radiation (bandwidth $\Delta\nu_{probe} \approx 0.3\ cm^{-1}$) was generated by resonant third-order sum−difference frequency conversion ($\nu_{probe} = 2\nu_R - \nu_T$) of pulsed dye laser radiation (pulse duration ≈ 15 ns) in a phase-matched Kr/Ar mixture.[30] In the four-wave mixing process, the frequency ν_R (λ_R = 212.55 nm) is two-photon resonant with the Kr 4p−5p ($^1/_2$, 0) transition. The frequency ν_T could be tuned from 844 to 848 nm to cover the H and D atom Lyman-α transitions ($\lambda_{L\alpha-H}$ = 121.567 nm, $\lambda_{L\alpha-D}$ = 121.534 nm). The generated VUV probe laser radiation was separated from the unconverted laser radiation by a lens monochromator. The VUV probe beam was aligned to overlap the photolysis beam at right angles in the viewing region of an LIF detector. H and D atom LIF signals were measured through a band-pass filter by a solar blind photomultiplier positioned at right angles to both photolysis and probe laser. The delay time Δt between the photolysis and the probe pulse was controlled by a pulse generator. The VUV-probe laser beam intensity was monitored after passing through the reaction cell with an additional solar blind photomultiplier. The LIF signal, the VUV-probe beam intensity, and the photolysis laser intensity were recorded with a boxcar system and transferred to a microcomputer where the LIF signal was normalized to both photolysis and probe laser intensities. To obtain a satisfactory *S*/*N* ratio, each point of the H and D atom Doppler profiles (Figure 1) was averaged over 30 laser shots. All measurements were carried out at a repetition rate of 6 Hz.

As in our previous studies of the H + D_2O → D + HOD hydrogen exchange reaction,[31] it was observed that the Lyman-α probe beam itself produced D atoms via photolysis of the DCl reagent alone. To distinguish these "background" D atoms from the D atoms produced by the H + DCl reaction, an electronically controlled mechanical shutter was inserted into the photolysis beam path. At each point of the D atom line scan, the signal was first averaged with the shutter opened and again averaged with the shutter closed. A point-by-point subtraction procedure was adopted to obtain on-line a signal free from background D atoms. The background subtraction method described above was also applied when H atom lines were recorded. Hence, all the data presented in the following are free from any contribution due to H_2S and DCl "Lyman-α self-photolysis". At this point, it should be mentioned that, in measurements where only DCl was present, no D atoms produced by the photolysis laser beams could be detected. In the flowing H_2S/DCl mixture, however, we observed a D atom background (see section III) which we attribute to direct photolysis of D_2S or HDS formed by a heterogeneous isotope exchange reaction at the walls of the mixing part of the flow system. In separate experiments, this D atom background was found to be independent of delay time and to decrease slowly when the flow of DCl was stopped, but on a time scale long enough to allow reliable determination of the Doppler profile of reactively produced D atoms by determining the difference between D atom profiles recorded with and without the presence of DCl. The D atom Doppler profile line shapes recorded without DCl flow were evaluated to determine the average kinetic energy, which was found to be consistent with D atom generation via 248 and 222 nm photolysis of D_2S or HDS, respectively.

III. Results

A. Single Collision Absolute Reaction Cross-Sections. Single collision cross-sections were obtained using the pulsed laser pump/probe method, which we have employed previously to measure absolute reaction cross-sections for the H + D_2O → D + HOD hydrogen atom exchange reaction.[27,31] The determination of absolute reactive cross-sections σ_R was based on the following equation:[31]

$$[D]_{\Delta t} = \sigma_R(E_{c.m.})v_{rel}[DCl][H]\Delta t + [D]_0 \qquad (5)$$

Here, v_{rel} is the relative velocity, $E_{c.m.} = {}^1/_2\mu v_{rel}^2$, of the reactants where μ represents the reduced mass of the H−DCl collision pair. $E_{c.m.}$ and hence v_{rel} can be calculated from the photolysis laser wavelength, the H−SH bond dissociation energy, and the internal state distribution of the SH fragment[29] as described in detail in ref 32. Δt stands for the time delay between the photolysis and probe laser pulses, which was determined by measuring the time difference between photolysis and probe scattered light pulses observed on a fast oscilloscope. [*x*] denotes the concentration of species *x* and $[D]_0$ the constant D atom background originating from the direct photolysis of D_2S/HDS formed by heterogeneous isotope exchange between H_2S and DCl as discussed in the previous section. After rewriting eq 5 as

$$[D]_{\Delta t}/[H] = \sigma_R(E_{c.m.})v_{rel}[DCl]\Delta t + [D]_0/[H] \qquad (6)$$

it can be seen that by measuring D/H atom ratios at different delay times Δt under identical experimental conditions, σ_R can be determined from the slope of a linear fit if the relative velocity and the DCl concentration are known. In Figure 1, H atom and D atom Doppler profiles observed when a room-temperature mixture of H_2S and DCl was irradiated by laser light with a wavelength of 222 nm (Figure 1a) and 248 nm (Figure 1b) are depicted. The H atom Doppler profiles shown in Figure 1a,b correspond to translationally excited H atoms with average collision energies of $E_{c.m.}$ = 1.4 eV and $E_{c.m.}$ = 1.0 eV, respectively. In a number of experimental runs, integrated areas under the H and D Doppler profiles were determined at various delay times. In Figure 2, a typical plot of the measured D/H atom ratios versus delay time is shown. Evaluation of the experimental data sets via eq 6 yielded absolute reaction cross-sections of $\sigma_R(1.4\ eV.) = 0.45 \pm 0.11$ Å^2 and $\sigma_R(1.0\ eV.) = 0.12 \pm 0.04$ Å^2 for the H + DCl → HCl + D exchange reaction.

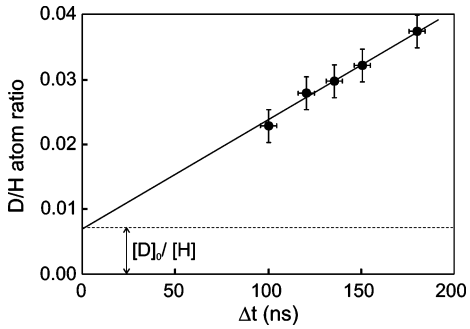

Figure 2. Plot of measured D/H atom ratios against delay time Δt between photolysis and probe laser pulse. H atoms were generated via pulsed 222 nm laser flash photolysis of H_2S in a flowing mixture of H_2S and DCl at a total pressure of 100 mTorr. $[D]_0$ stands for the photolytically produced D atom background (for details, see text and ref 31).

B. Excitation Function and Reaction Threshold Determination. If translationally excited H atoms are generated by pulsed laser photolysis of H_2S molecules in a large excess of a moderator gas, the initially present nascent nonequilibrium H atom velocity distribution evolves toward the thermal equilibrium distribution determined by the temperature of the moderator gas. Therefore, the velocity distribution of the H atoms in the laboratory frame has to be described by a time-dependent distribution function (see, e.g., ref 33 and references therein). When a reagent, such as DCl, is present, reactive collisions occur in competition with the translational relaxation. In this case, the nonequilibrium kinetics of D atom product formation in the moderated hot H atom reaction H + DCl → HCl + D are then described by the rate equation[27]

$$\frac{\mathrm{d}[\mathrm{D}]_t}{\mathrm{d}t} = \{\int_0^\infty \sigma_R(v_{rel}) v_{rel} f(v_{rel}, t)\, \mathrm{d}v_{rel}\}[\mathrm{H}]_t[\mathrm{DCl}] \quad (7)$$

Here, it has been assumed that DCl is present in excess over H atoms so that its concentration remains constant in time. $f(v_{rel}, t)$ stands for the time-dependent distribution function of the reagents' relative velocities in the H−DCl collision frame. In eq 7, the term in braces represents the reaction rate constant which, under the translationally nonequilibrium conditions of the present experiments, is time-dependent. After replacing $[H]_t$ by $[H]_{t=0} - [D]_t$ and introducing the new variable $\chi_D(t) = [D]_t/[H]_{t=0}$, which represents the fractional yield of D atoms produced, the following expression can be obtained as a solution of eq 7 for the initial condition $\chi_D(t = 0) = 0$:

$$\chi_D(\Delta t) = [\mathrm{DCl}] \int_0^{\Delta t} \{\int_0^\infty \sigma_R(v_{rel}) v_{rel} f(v_{rel}, t)\, \mathrm{d}v_{rel}\}[1 - \chi_D(\Delta t)]\, \mathrm{d}t \quad (8)$$

In eq 8, the delay time Δt between the pump laser pulse, which generates the H atom reagents, and the probe laser pulse, which detects the D atom products, corresponds to the reaction time. To perform the integration in eq 8, one has to know the excitation function, i.e., the reaction cross-section σ_R as a function of the relative velocity, as well as the time dependence of the relative velocity distribution function $f(v_{rel}, t)$. On the other hand, when $\chi_D(\Delta t)$ and $f(v_{rel}, t)$ can be determined experimentally, information about the actual form of the excitation function can be obtained.

The pulsed laser pump/probe method employed in the present work allowed the direct determination of both the D atom product yield $\chi_D(\Delta t)$ and the time-dependent relative velocity distribution function $f(v_{rel}, t)$. $\chi_D(\Delta t)$ could be obtained from the ratio of the integrated areas of the D atom products measured at reaction time Δt (see, e.g., Figure 3) and the nascent H atom reagent Doppler profile measured at a reaction time close to zero (before significant reaction could occur).

As described in detail in ref 27, the H atom Doppler line shapes measured at different pump/probe delay times were evaluated to determine the laboratory frame distribution $f(v_z, t)$ of the velocity component v_z of the absorbing H atoms along the propagation direction of the probe laser beam. A symmetric double sigmoidal function, eq 9, was used as a fitting function to evaluate the measured H atom Doppler line shape, as it well describes the Doppler line shapes at both short and long pump−probe delay times (see Figure 3a). In eq 9, A is a normalization

$$f(v_z, t) = A\left[\frac{1}{1 + \exp\left\{-\dfrac{[v_z + \omega_1(t)/2]}{\omega_2(t)}\right\}}\right]\left[1 - \frac{1}{1 + \exp\left\{-\dfrac{[v_z - \omega_1(t)/2]}{\omega_2(t)}\right\}}\right] \quad (9)$$

factor, while the two variables $\omega_1(t)$ and $\omega_2(t)$ are a measure for the time-dependent width of the profile and the steepness of its wings, respectively. To derive an empirical representation of $f(v_z, t)$, ω_1 and ω_2 were parametrized by the following functions:

$$\omega_1(t) = a_1 + b_1 \exp(-c_1 t) \quad (10)$$

$$\omega_2(t) = a_2 + b_2\sqrt{t} \exp(-c_2 t) \quad (11)$$

In Figure 4, the solid lines represent the results of a least-squares fit of the measured data, which was used to determine the functional forms of $\omega_1(t)$ and $\omega_2(t)$ under the conditions of the present experiments.

In Figure 3a, H atom Doppler profiles, which were simulated using eq 9 as the empirical representation of $f(v_z, t)$, are depicted as solid lines and compared to the experimental ones (solid circles). The corresponding time-dependent distribution function $f(v_{rel}, t)$ obtained from $f(v_z, t)$ by differentiation followed by a laboratory to center-of-mass transformation (for details, see refs 32 and 33) is depicted in Figure 3b. Doppler profiles of the D atom reaction products are shown in Figure 3c. Values for the reaction times at which the respective H and D atom Doppler profiles were recorded are given in the figure.

In Figure 5, results of a D atom fractional product yield measurement are plotted against the reaction time. The experimental data were analyzed by assuming a model excitation function given by eq 12 containing parameters a, b, and c to be optimized.

$$\sigma_R(E_{c.m.}) = \begin{cases} a + bE_{c.m.} + cE_{c.m.}^2 & \text{for } E_{c.m.} \geq E_0 \\ 0 & \text{for } E_{c.m.} < E_0 \end{cases} \quad (12)$$

With the time-dependent parametrization of the H−DCl reagents' relative velocity distribution function $f(v_{rel}, t)$, D atom fractional yields predicted by the model excitation function could be calculated via eq 8 for the conditions corresponding to each measured data point $\chi_D(\Delta t)$. The integration over t in eq 8 was performed numerically. A measure of the quality of a given set of excitation function parameters could be obtained by computing the global mean-squared deviation of both the nonequilibrium kinetics data set and the single collision cross-sections from the corresponding values calculated from the trial excitation function. Optimization of the excitation function parameters a,

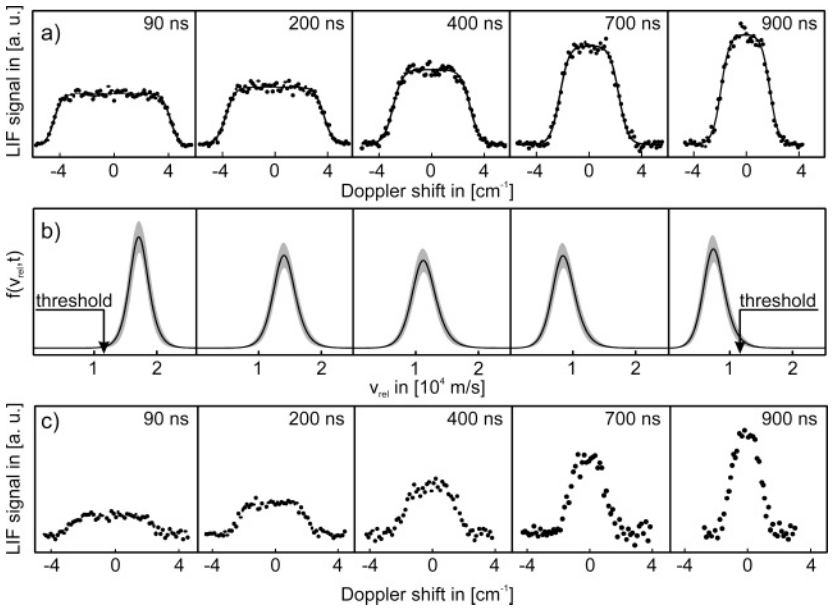

Figure 3. (a) H atom Doppler profiles measured at different pump−probe delay times between 90 and 900 ns after 222 nm laser flash photolysis of 10 mTorr of H_2S in a flowing mixture of 80 mTorr of DCl and 1 Torr of Ar. Solid lines are results of a nonlinear least-squares fit analysis of the measured Doppler profiles performed to determine the time evolution of the H atom laboratory velocity distribution $f(v_z, t)$ as described in the text. (b) Evolution of the corresponding time-dependent distribution function $f(v_{rel}, t)$ of the relative velocity in the H−DCl collision frame. Shaded areas represent 1σ statistical uncertainty determined by simple error propagation from the least-squares fit procedure employed to derive a continuous analytical representation for the time evolution of the line shape parameters $\omega_1(t)$ and $\omega_2(t)$ (solid lines in Figure 4). The arrows mark the threshold for the H + DCl → HCl + D reaction. (c) Doppler profiles of D atoms produced in the reaction H + DCl → HCl + D. The D atom signal at 900 ns corresponds to a D atom product yield of $\chi_D(900\text{ ns}) = [D]_{900\text{ ns}}/[H]_{t=0} \approx 0.04$.

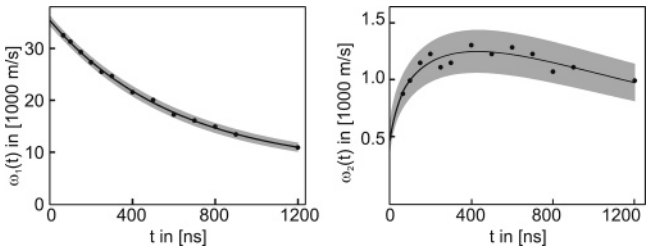

Figure 4. Measured time dependence of the H atom Doppler profile line shape parameters ω_1 and ω_2 (solid circles). Experimental conditions are the same as in Figure 3. Solid lines are the results of a least-squares fit procedure used to derive a continuous analytical representation for the two parameters $\omega_1(t)$ and $\omega_2(t)$. Shaded areas represent 1σ statistical uncertainty of the respective fitting function.

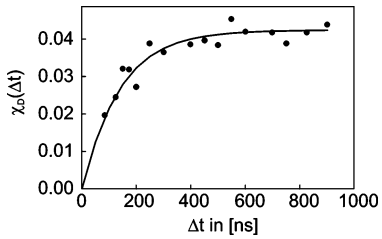

Figure 5. Plot of the D atom product yield χ_D versus reaction time. Filled circles represent experimental results. The solid line is the result of a simulation of the experimental moderation conditions using the measured velocity distribution $f(v_{rel}, t)$ and the excitation function $\sigma_R(E_{c.m.})$ reproduced in Figure 6 as a solid line.

b, and *c* was performed by a nonlinear least-squares fit to minimize the sum of these two mean-squared deviations. The latter procedure yielded a set of optimal values resulting in the excitation function depicted in Figure 6 as a solid line, which corresponds to a reaction threshold energy of $E_0 = 0.65 \pm 0.13$ eV. The statistical uncertainty in each of the model parameters allows estimation of the confidence region (1σ) of the excitation function, which is shown as the shaded area in Figure 6.

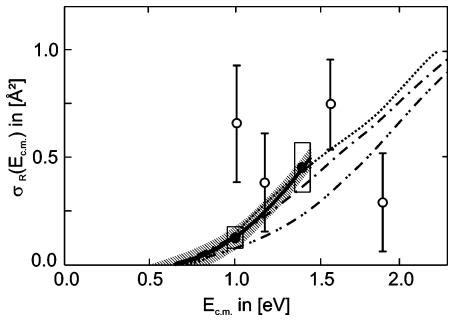

Figure 6. Comparison between experimental and theoretical absolute reaction cross-sections for the H + DCl → HCl + D hydrogen atom exchange reaction. Open circles are experimental results obtained by Polanyi and co-workers.[16] The filled circles are the experimental results of the present single collision reaction cross-section measurements, where the widths of the boxes drawn around represent the spreads (fwhm) in the collision energy distributions, and the heights of the boxes represent the experimental uncertainties of the measurements. The solid line is the excitation function $\sigma_R(E_{c.m.})$ derived in the present moderated hot H atom experiments. The shaded area reflects the statistical uncertainty (1σ) of the least-squares fit procedure used to determine the optimum excitation function (for details, see text). Theoretical excitation functions obtained in quasiclassical trajectory calculations[12] performed on different potential energy surfaces (PESs): "dotted" curve, BW2-PES; "dash−dot" curve, BW1-PES; "dash−dot−dot" curve, G3-PES.

IV. Discussion

In Figure 6, the global excitation function derived in the present moderated hot H atom study of the H + DCl → HCl + D reaction is depicted (solid line) along with the two single collision reaction cross-sections $\sigma_R(1.0\text{ eV}) = 0.12 \pm 0.04$ Å^2 and $\sigma_R(1.4\text{ eV}) = 0.45 \pm 0.11$ Å^2 (filled circles) obtained in the course of the present work. The width of the boxes drawn around the latter quantities represents the spread (fwhm) in the nascent collision energy distribution,[32] and the height of the

boxes represents the experimental uncertainties in the reaction cross-measurements.

For comparison with the experiments, results obtained in QCT calculations[12] on the G3 (dash−dot−dot curve) and on the BW1 (dash−dot curve) and BW2 (dotted curve) PESs are reproduced in Figure 6. The latter two PESs represent two slightly different versions of the PES of Bian and Werner,[5] which is based on extensive and high-quality ab initio calculations performed at 1200 geometries. The BW1 version is based on a global fit of the original ab initio data points, whereas the BW2 version was obtained by scaling the correlation energies at all geometries with a constant factor chosen in order to more accurately reproduce the HCl and H_2 bond dissociation energies.[5]

The theoretical excitation functions shown in Figure 6 represent rotationally averaged quantities. To account explicitly for the experimental conditions of the present work, the reactive cross-sections were averaged over a room-temperature Boltzmann distribution of the DCl reagent rotational levels in the ground vibrational state.[12] As discussed in refs 11 and 12, for all three PESs employed in the QCT calculations the influence of DCl reagent rotation on reactivity was found to be relatively small for all DCl rotational levels significantly populated at room temperature (see, e.g., Figure 2 in ref 11) resulting in virtually temperature independent rotationally averaged reaction cross-section values for $T_{rot(DCl)} \leq 300$ K. Hence, a further comparison of the QCT results with absolute reaction cross-sections obtained by Polanyi and co-workers (depicted as open circles in Figure 6)[16] in experiments with "cold" DCl reagent molecules with a rotational temperature of ca. 30 K[11] is possible. However, as can be seen in Figure 6, the earlier experimental results, with values between 0.25 and 0.75 Å^2 for the depicted collision energy range, did not reveal any clear trend in the collision energy dependence of the exchange reaction cross-section. The experimental values of ref 16 seem to indicate a moderate decline of the excitation function for collision energies above 1.0 eV. Such a collision energy dependence of the reaction cross-section would however be at variance with the QCT excitation functions, all of which exhibit a strictly monotonic increase from the reaction threshold to a value of ca. 1 Å^2 at a collision energy of $E_{c.m.} = 2.25$ eV.[12] The BW2 cross-sections are slightly larger than the BW1 ones because of the slightly higher barrier for the exchange reaction on the latter PES.[5] The G3 excitation function, although qualitatively similar in shape to the excitation functions obtained on the BW surfaces, is significantly smaller in absolute value for collision energies above ca. 0.9 eV.

In contrast to the previous experimental results,[16] the excitation function obtained in the present study (solid line in Figure 6) exhibits an energy dependence in accordance with theory. In addition, the experimentally obtained reaction threshold energy of $E_0 = 0.65 \pm 0.13$ is in good agreement with the joint theoretical threshold energy of $E_0 \approx 0.65$ eV reported in ref 12. A detailed inspection of Figure 6 reveals that for low collision energies ($E_{c.m.} < 1.0$ eV) all three PESs yield cross-sections which agree, within the experimental uncertainty (represented by the shaded area in Figure 6), with the excitation function $\sigma_R(E_{c.m.})$ derived in the present moderated hot H atom experiments. For collision energies above ca. 1.0 eV, however, the G3 cross-sections fall below the lower error limit of the experimental excitation function, while both the BW1 and BW2 cross-sections continue to lie within the experimental error bounds up to a collision energy of about 1.3 eV. For the highest collision energies employed in the present experiments, however, only the BW2 excitation function continues to agree with the experimental one, demonstrating that within the framework of the QCT approach of ref 12 the latter PES provides at present the most accurate description of the dynamics of the H + DCl → HCl + D exchange reaction 4.

Caution should be taken, however, to draw a final conclusion about the comparative quality of the BW2 and G3 PESs in regard to the ability to accurately describe the dynamics of both the exchange and abstraction reactions in the low as well as high collision energy regimes. The BW2 PES was particularly successful in reproducing experimental results such as, e.g., the collision energy dependence of the DCl/HCl branching ratio for the Cl + HD reaction measured by Liu and co-workers, which could not be reproduced in QMS calculations on the G3 PES.[34] Because of the relatively low collision energies $E_{c.m} = 0.17-0.35$ eV employed, however, only the barrier region and the entrance valley features of the respective abstraction reaction pathways on the BW2 and G3 PESs were probed in the latter studies.

Experimental investigations of the abstraction reactions 1 and 3, in which translationally excited H atoms were employed to study the reaction dynamics in the higher collision energy regime $E_{c.m} = 1.0-2.4$ eV,[12,15−17] yielded reaction cross-sections which were considerably smaller than the respective reaction cross-sections obtained in QCT calculations on the BW2 PES.[12] In particular, for the H + DCl → HD + Cl abstraction reaction 3, the absolute values of the experimental reaction cross-sections and their collision energy dependence[16,17] were found to be in good agreement with QCT results obtained on the G3 surface,[11] which yielded cross-sections that were smaller than the BW2 cross-sections[12] by a factor of about 2 (see, e.g., figure 4 of ref 17). A detailed discussion concerning the origin of the large difference in reactivity observed in the QCT calculations on the BW2 and G3 PESs at high H + DCl collision energies is given ref 12, where, e.g., individual high-energy trajectories were analyzed in combination with $R-\gamma$ contour plots of the two PESs (here, R denotes the distance between the incoming H atom and the center-of-mass of the DCl reactant, and γ is the Jacobi angle between R and the DCl internuclear distance). In this empirical analysis, narrow "valleys" in the contour plot centered at $\gamma \approx 30°$, which are not present in the G3 PES, were identified as the most probable origin of the too-high reactivity of the abstraction reaction on the BW2 PES. In addition, it has been noted that, because of the purely adiabatic character of the QCT calculations,[11,12] nonadiabatic effects, such as the formation of spin−orbit excited Cl*($^2P_{1/2}$) atom products via a Born−Oppenheimer forbidden reactive pathway, which was experimentally observed in the abstraction reactions 1 and 3 at higher collision energies,[12,17] could not be accounted for. Hence, the need for more sophisticated reactive scattering calculations beyond the single-surface approach of ref 12 is clearly obvious for a more comprehensive description of the dynamical features of the abstraction reactions. However, considering the recent efforts undertaken to develop coupled ab initio PESs[25] to study spin−orbit and nonadiabatic effects in the Cl + H_2 reaction,[21,35,36] it is not unreasonable to expect that multisurface scattering calculations for the H + HCl/DCl → H_2/HD + Cl abstraction reactions will soon be within reach.

V. Summary

In the present work, a moderated hot H atom pulsed laser "pump-and-probe" approach, based on a combination of single collision reaction cross-section, H atom moderation, and non-equilibrium D atom formation rate measurements,[27] was applied to determine the reaction threshold and a global representation of the rotationally averaged excitation function $\sigma_R(E_{c.m.})$ for the

H + DCl → HCl + D hydrogen atom exchange reaction. In contrast to the results of previous reaction cross-section measurements,[16] the excitation function obtained in the present study exhibits an energy dependence in accordance with theory. Detailed comparison with results of dynamics calculations performed on three different PESs showed that a single-surface QCT approach[11,12] using the high-quality BW2 ab initio ground-state PES of Bian and Werner[5] can accurately reproduce the present experimental results, indicating that the exchange reaction occurs adiabatically on the ground-state PES. The latter finding contrasts with that of our previous dynamics studies of the H + HCl/DCl → H_2/HD + Cl abstraction reactions,[12,17] which demonstrated that for these reactions nonadiabatic (Born−Oppenheimer forbidden) reactive pathways, leading to the formation of spin−orbit excited Cl*($^2P_{1/2}$) products, play a significant role at higher collision energies.

Acknowledgment. This work was supported by the Deutsche Forschungsgemeinschaft (DFG). A.L. was supported by the Landesgraduierten-Förderung Baden-Württemberg. R.K.V. thanks DLR Bonn for a fellowship under the Indo-German bilateral agreement. J.P.M. gratefully acknowledges the financial support received by the Humboldt foundation through a Humboldt research award.

References and Notes

(1) Bodenstein, M.; Dux, W. *Z. Phys. Chem.* **1913**, *85*, 297.
(2) See, e.g., Laidler, K. J. *Chemical Kinetics*, 3rd ed.; Harper & Row: New York, 1987, and references therein.
(3) See, e.g., Allison, T. C.; Mielke, S. L.; Schwenke, D. W.; Lynch, G. C.; Gordon, M. S.; Truhlar, D. G. *Gas-Phase Chemical Reaction Systems: Experiments and Models 100 Years after Max Bodenstein*; Springer Series in Chemical Physics Vol. 61; Wolfrum, J., Volpp, H.-R., Rannacher, R., Warnatz, J., Eds.; Springer: Heidelberg, 1996.
(4) Allison, T. C.; Lynch, G. C.; Truhlar, D. G.; Gordon, M. S. *J. Phys. Chem.* **1996**, *100*, 13575, and references therein.
(5) Bian, W.; Werner, H.-J. *J. Chem. Phys.* **2000**, *112*, 220.
(6) Atkinson, R.; Baulch, D. L.; Cox, R. A.; Hampson, R. F., Jr.; Kerr, J. A.; Rossi, M. J.; Troe, J. *J. Phys. Chem. Ref. Data* **1997**, *26*, 521, and references therein.
(7) Kumaran, S. S.; Lim, K. P.; Michael, J. V. *J. Chem. Phys.* **1994**, *101*, 9487; Michael, J. V. in ref 3.
(8) Mielke, S. L.; Allison, T. C.; Truhlar, D. G.; Schwenke, D. W. *J. Phys. Chem.* **1996**, *100*, 13588.
(9) Aoiz, F. J.; Bañares, L. *J. Phys. Chem.* **1996**, *100*, 18108.
(10) Wang, H.; Thompson, W. H.; Miller, W. H. *J. Chem. Phys.* **1997**, *107*, 7194.
(11) Aoiz, F. J.; Herrero, V. J.; Sáez Rábanos, V.; Tanarro, I.; Verdasco, E. *Chem. Phys. Lett.* **1999**, *306*, 179.
(12) Aoiz, F. J.; Bañares, L.; Bohm, T.; Hanf, A.; Herrero, V. J.; Jung, K.-H.; Läuter, A.; Lee, K. W.; Menéndez, M.; Sáez Rábanos, V.; Tanarro, I.; Volpp, H.-R.; Wolfrum, J. *J. Phys. Chem. A* **2000**, *104*, 10452.
(13) Yao, L.; Han, K.-L.; Song, H.-S.; Zhang, D.-H. *J. Phys. Chem. A* **2003**, *107*, 2781.
(14) Aker, P. M.; Germann, G. J.; Valentini, J. J. *J. Chem. Phys*. **1989**, *90*, 4795.
(15) Brownsword, R. A.; Kappel, C.; Schmiechen, P.; Upadhaya, H. P.; Volpp, H.-R. *Chem. Phys. Lett.* **1998**, *289*, 241.
(16) Barclay, V. J.; Collings, B. A.; Polanyi, J. C.; Wang, J. H. *J. Phys. Chem.* **1991**, *95*, 2921.
(17) Hanf, A.; Läuter, A.; Suresh, D.; Volpp, H.-R.; Wolfrum, J. *Chem. Phys. Lett.* **2001**, *340*, 71.
(18) Lee, S.-H.; Liu, K. *J. Chem. Phys.* **1999**, *111*, 6253.
(19) Lee, S.-H.; Lai, L.-H.; Liu, K.; Chang, H. *J. Chem. Phys.* **1999**, *110*, 8229.
(20) Dong, F.; Lee, S.-H.; Liu, K. *J. Chem. Phys.* **2001**, *115*, 1197.
(21) Alexander, M. H.; Capecchi, G.; Werner, H.-J. *Science* **2002**, *296*, 715.
(22) Schatz, G. C. *J. Phys. Chem*. **1995**, *99*, 7522.
(23) Balucani, N.; Skouteris, D.; Cartechini, L.; Capozza, G.; Segoloni, E.; Casavechia, P.; Alexander, M. H.; Capecchi, G.; Werner, H.-J. *Phys. Rev. Lett.* **2003**, *91*, 13201.
(24) Balucani, N.; Skouteris, D.; Capozza, G.; Segoloni, E.; Casavechia, P.; Alexander, M. H.; Capecchi, G. Werner, H.-J. *Phys. Chem. Chem. Phys.* **2004**, *6*, 5007.
(25) Capecchi, G.; Werner, H.-J. *Phys. Chem. Chem. Phys.* **2004**, *6*, 4975.
(26) Schwenke, D. W.; Tucker, S. C.; Steckler, R.; Brown, F. B.; Lynch, G. C.; Truhlar, D. G.; Garrett, B. C. *J. Chem. Phys.* **1989**, *90*, 3110.
(27) Brownsword, R. A.; Hillenkamp, M.; Laurent, T.; Volpp, H.-R.; Wolfrum, J.; Vatsa, R. K.; Yoo, H.-S. *J. Phys. Chem.* **1997**, *101*, 6448.
(28) Brownsword, R. A.; Hillenkamp, M.; Laurent, T.; Vatsa, R. K.; Volpp, H.-R. *J. Chem. Phys.* **1997**, *106*, 4436.
(29) Continetti, R. E.; Balko, B. A.; Lee, Y. T. *Chem. Phys. Lett.* **1991**, *182*, 400.
(30) Hilbert, G.; Lago, A.; Wallenstein, R. *J. Opt. Soc. Am. B* **1987**, *4*, 1753.
(31) Brownsword, R. A.; Hillenkamp, M.; Laurent, T.; Vatsa, R. K.; Volpp, H.-R.; Wolfrum, J. *Chem. Phys. Lett.* **1996**, *259*, 375.
(32) v. d. Zande, W. J.; Zhang, R.; Zare, R. N.; Valentini, J. J. *J. Phys. Chem.* **1991**, *95*, 8205.
(33) Park, J.; Shafer, N.; Bersohn, R. *J. Chem. Phys.* **1989**, *91*, 7861.
(34) Skouteris, D.; Manolopoulos, D. E.; Bian, W.; Werner, H.-J.; Lai, L.-H.; Liu, K. *Science* **1999**, *286*, 1713.
(35) Skouteris, S.; Laganà, A.; Capecchi, G.; Werner, H.-J. *Phys. Chem. Chem. Phys.* **2004**, *6*, 5000.
(36) Manthe, U.; Capecchi, G.; Werner, H.-J. *Phys. Chem. Chem. Phys.* **2004**, *6*, 5026.